Journal of Marine Research, 61, 147–173, 2003

Journal of
MARINE RESEARCH

Volume 61, Number 2

On the generation of North Brazil Current rings

by Markus Jochum[1] and Paola Malanotte-Rizzoli[1]

ABSTRACT

A high resolution general circulation model (OGCM) is used to investigate the life cycle of North Brazil Current (NBC) rings. The focus of the study is on explaining the generation mechanisms of the rings and their vertical structure. The OGCM is used in a configuration simplified as much as possible but capable of reproducing a realistic mean circulation of the tropical Atlantic.

Three numerical experiments are analyzed: no wind; steady wind; seasonally varying winds. With wind forcing, a consistent scenario emerges for the generation of NBC rings. It is shown first that the NECC is barotropically unstable, radiating Rossby waves of the first baroclinic mode with a period of 63 days (steady wind) or 50 days (variable wind). These waves reflect at the Brazilian coast and create about 6–7 anticyclones per year. These anticyclones intensify as they propagate northwestward along the Brazilian coast because of potential vorticity conservation and become NBC rings. Among them, about one per year reaches a depth below 1000 m. These deep rings are created by the merger of a surface NBC ring with an intermediate eddy. The intermediate eddies are produced by the Intermediate Western Boundary Current (IWBC) which becomes unstable upon crossing the equator.

1. Introduction

Since their first description a decade ago (Johns *et al.,* 1990; Didden and Schott, 1993), North Brazil Current (NBC) rings have received increasing attention. First, the mechanisms governing their generation, detachment and propagation pose a very interesting dynamical problem. Second, NBC rings may constitute an important component of the upper limb return flow of the meridional overturning circulation (MOC) by contributing to the northward transport of southern Atlantic water into the northern subtropical gyre.

1. Department of Earth, Atmospheric and Planetary Sciences, MIT, Cambridge, Massachusetts, 02138, U.S.A.
email: markus@ocean.mit.edu

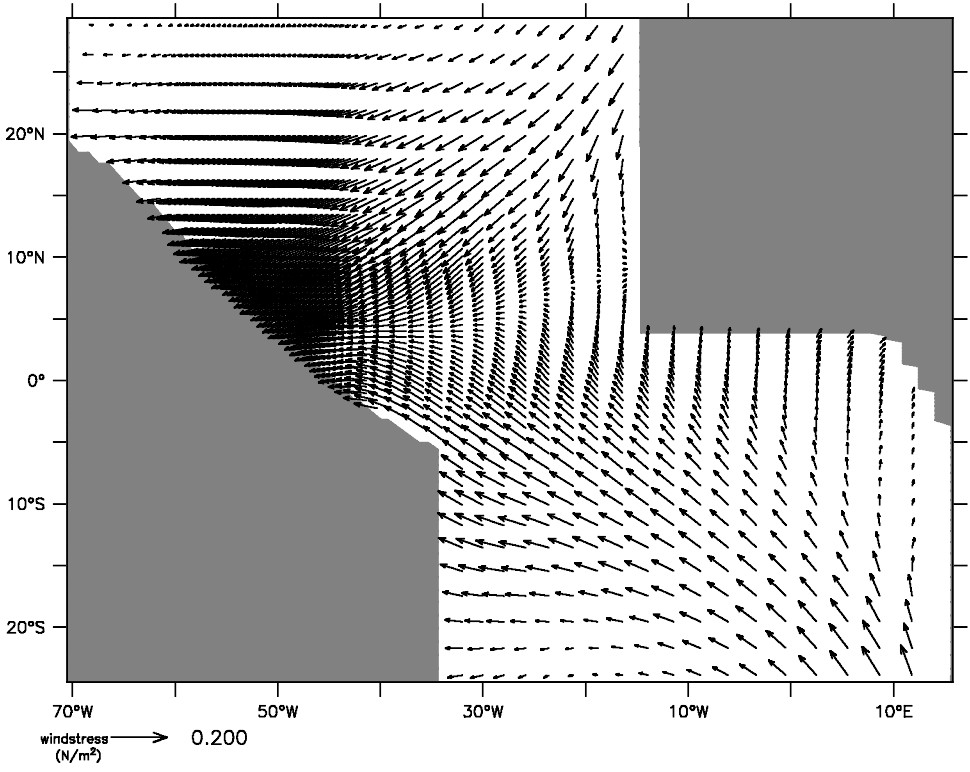

Figure 1. The yearly mean wind stress over the domain. The pattern shows the high resolution along the Brazilian coast and the equator (only every fourth gridpoint is shown). The Caribbean Sea is not part of the model domain.

The NBC rings are shed at the western boundary of the tropical Atlantic where the NBC forms a strong meander that retroflects into the North Equatorial Countercurrent (NECC). After separating from the retroflection region, the rings travel northwestward along the Brazilian coast. Their relevance for the northward transport of South Atlantic water clearly depends on their frequency of generation as well as on their horizontal and vertical structure.

Being generated by the NBC, the rings are one of the major components of the complex tropical Atlantic current system. Observationally, it is rather difficult to define a mean tropical Atlantic circulation because of the strong seasonal signal superimposed on the annual mean (Johns *et al.,* 1998; Schott *et al.,* 1998). Even in the standard mean scenario commonly accepted, *in situ* observational evidence of the ring birth and structure is difficult to obtain through traditional measurements because of the high variability of the retroflecting meander and detachment region. Satellite observations are mostly descriptive in nature, possibly providing a census of the rings over time but no information about their three-dimensional structure.

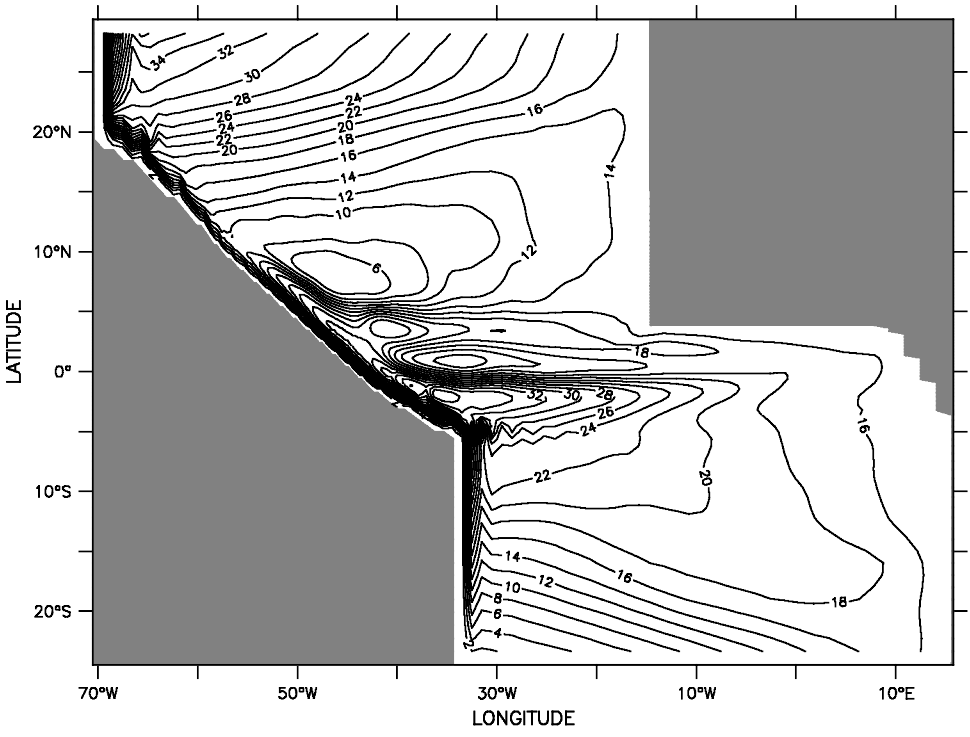

Figure 2. The annual mean barotropic transport streamfunction (in Sv).

Theoretically, it is also difficult to apply traditional approaches to study the instability of the NBC because of its proximity to the western boundary and its nonzonal nature (Pedlosky, 1979). Finally, the jet-like structure of the NBC and the nature of the ring formation make the process a highly nonlinear one (see however da Silveira *et al.* (2000) for a quasi-geostrophic study). A possible approach to study the dynamics of the NBC rings is to use an ocean general circulation model (OGCM) in a configuration as simplified as possible that reproduces the basic observational features of the equatorial current system, of the NBC and of the rings. In the present investigation we follow such an approach, focusing on the following two major questions:

- Which are the dynamical mechanisms responsible for NBC ring generation and detachment?
- How can their vertical structure be explained?

The paper is organized as follows. In Section 2 the model configuration is described and comparisons are made between the mean properties of the simulated circulation and the observational evidence. In Section 3 the numerical experiments are discussed and results are shown aimed to provide answers to the above questions. Section 3 is divided into three parts, discussing respectively the results of the simulations, the role of the NECC, and the

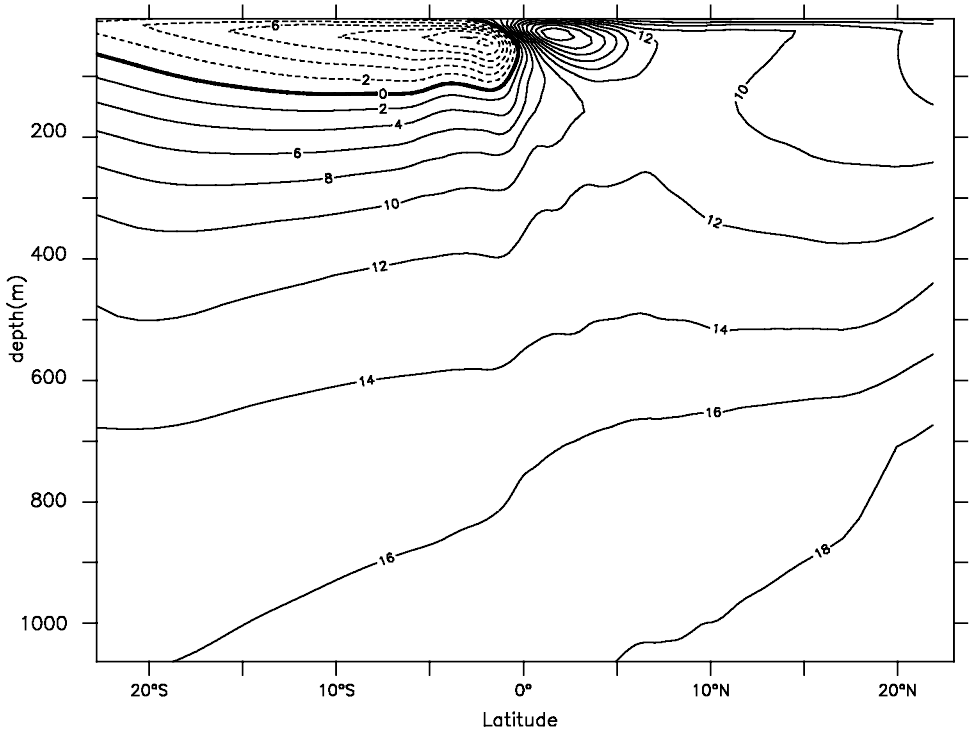

Figure 3. The annual mean zonally integrated transport streamfunction in the upper 1000 m of the water column (contour interval: 2 Sv).

deep structure of the rings. Finally, in Section 4, an overall discussion is provided summarizing the major novel results.

2. The model configuration

The model used is the MOM2b version of the GFDL-OGCM. The model configuration is an idealized basin from 25S to 30N in latitude and from 70W to 15E in longitude, with a flat bottom at 3000 m. The resolution is 1/4° by 1/4° at the western boundary between the equator and 12N, becoming coarser toward the eastern, northern and southern boundaries. The latitudinal resolution is reduced from 1/4° to 1° at the meridional boundaries, and the longitudinal resolution is reduced from 1/4° to 1.5° at the eastern boundary. Figure 1 shows the model configuration and the variable resolution. Thirty levels are used in the vertical with 10 m resolution in the top 100 m.

Horizontal mixing is performed by a Laplacian scheme with eddy viscosity and diffusivity linearly dependent on the resolution: from 200 m^2s^{-1} for 1/4° to 2000 m^2s^{-1} for 1° resolution. In the vertical, a Richardson number-dependent vertical mixing scheme

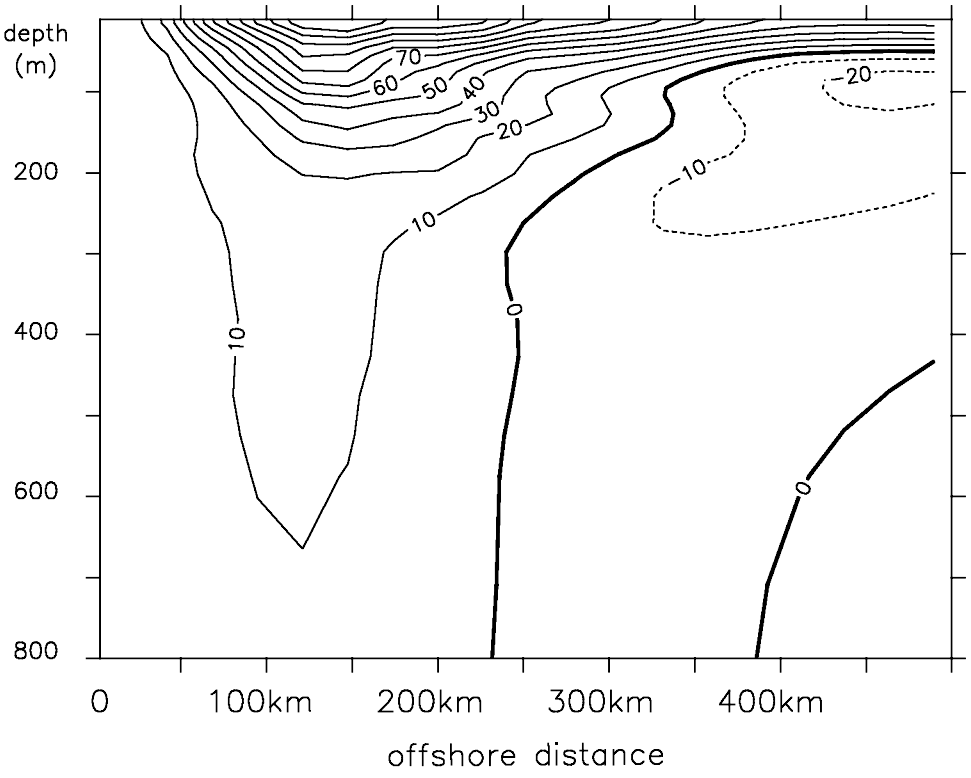

Figure 4. The simulated alongshore velocity at 4N averaged over 16 months as in Johns *et al.* (1998) (see his Fig. 9).

is used. Unstable temperature gradients are eliminated by mixing heat vertically to a depth that ensures a stable density gradient.

The initial condition is a state of rest. Salinity is kept constant in time and space at a value of 35 psu. The wind stress (Hellerman and Rosenstein, 1983) and the resulting depth integrated circulation are shown in Figure 1 and Figure 2, respectively. The anticyclonic circulations north of 18N and south of 10S will be referred to as northern and southern subtropical gyres (STGs). The cyclonic circulation between 5N and 18N will be called the tropical gyre (TG) and the equatorial gyre (EG) is between 10S and 5N. The initial temperature distribution is symmetric about the equator and is basically a zonally averaged, idealized climatology (as shown in Fig. 1 of Liu and Philander, 1995). This meridional profile is also used at the surface to restore the surface temperature with a 40-day relaxation time. The numerical simulation was integrated for 18 years before analyses were performed. The short spin-up time is due to the fast adjustment of the tropical circulation (Liu and Philander, 1995). The effect of the global MOC was represented by open boundary conditions (OBC). It is well known that OBC render the

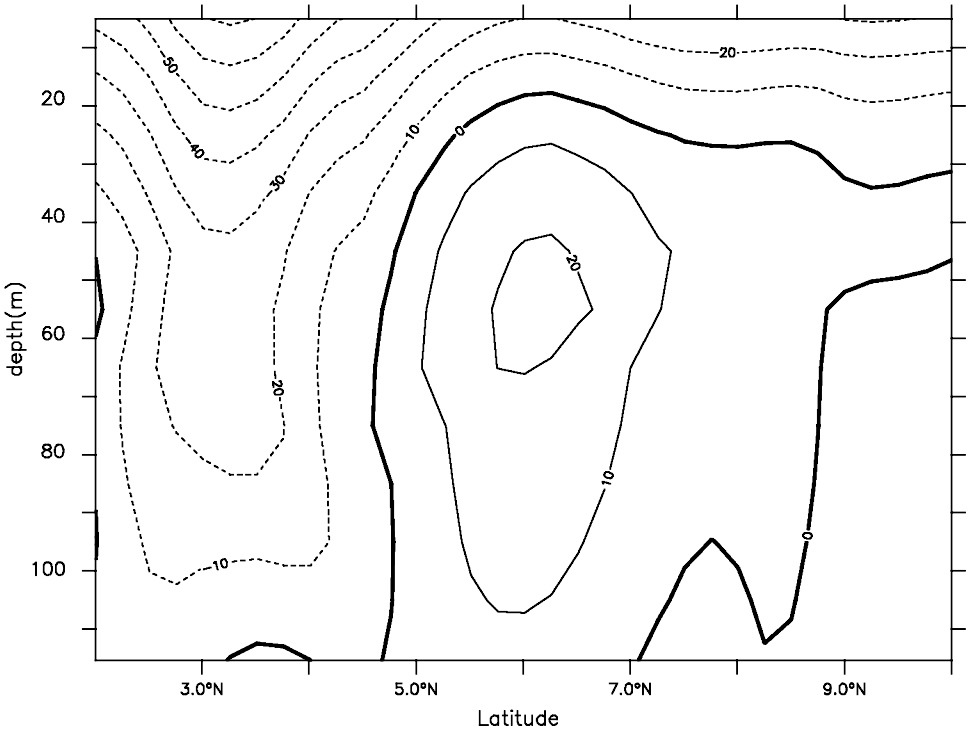

Figure 5. The zonal velocity across 38W in April (in cm/s). The eastward NECC can be seen at 6N, the westward South Equatorial Current at 3N, and the westward Ekman flow everywhere in the upper 20 m.

problem of solving the primitive equations ill posed (Oliger and Sundstrom, 1978). Nevertheless the simulations are reasonably accurate if the errors introduced by the OBC are small enough and do not grow in time (see Spall and Robinson (1989) for a detailed discussion). At the open boundaries temperatures and meridional velocities need to be specified. Furthermore, the tangential velocities of the inflow points have also to be defined, while at outflow points they can be calculated by assuming conservation of relative vorticity (Spall and Robinson, 1989).

The code used provides subroutines for OBC that were modified for our purposes. At the open boundaries the temperature and the barotropic streamfunction are specified. Using the Sverdrup balance and geostrophy the meridional velocity field is calculated (Stevens, 1990). The zonal velocity at the boundaries is zero. The barotropic streamfunction and temperature at the meridional boundaries are taken from the steady state solution of the purely wind-driven circulation simulated in a basin extending from 40S to 40N. To simulate the throughflow of the MOC return flow, the barotropic streamfunction is modified so that 15 Sv flow into the South Atlantic in the upper 1000 m all along the southern boundary and leave the North Atlantic in the northwest corner through a western

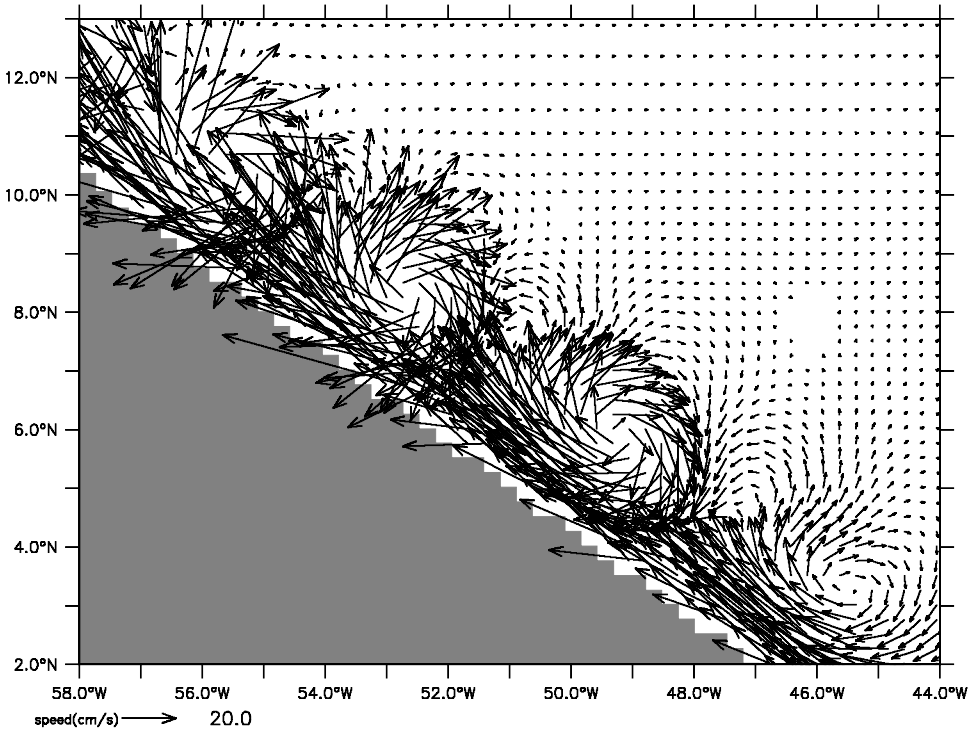

Figure 6. The flow field at the surface of the western tropical Atlantic in NW. One can see how the flow breaks up into eddies that travel north along the coast.

boundary current. For a discussion of the influence of the MOC for the tropical circulation see Jochum and Malanotte-Rizzoli (2001), even though it must be pointed out that the present manuscript describes rather different simulations.

The MOC inflow at the southern boundary and outflow in the western boundary current at the northern one are evident in Figure 2 that shows the time-mean, depth-integrated transport. Figure 3 shows the time-mean zonally integrated transport in the upper 1000 m. The southern subtropical cell in the southern hemisphere is evident, as well as the strong wind-induced equatorial cell at the equator and the throughflow of intermediate water below the thermocline. Thus, across each latitude there is a net northward transport of 15 Sv; the model dynamics determine at which depth, longitude and within which dynamical structure (boundary current, Ekman flow, vortices) this transport takes place. These 15 Sv are roughly consistent with the values available in the literature (Schmitz and McCartney, 1993). A deep western boundary current was not simulated, the focus being on the warm water return flow of the MOC and its interaction with the wind-driven circulation.

To gain confidence in the model's performance, the model results were compared with available observations. Figure 4 shows the mean alongshore velocity of the NBC at 4N.

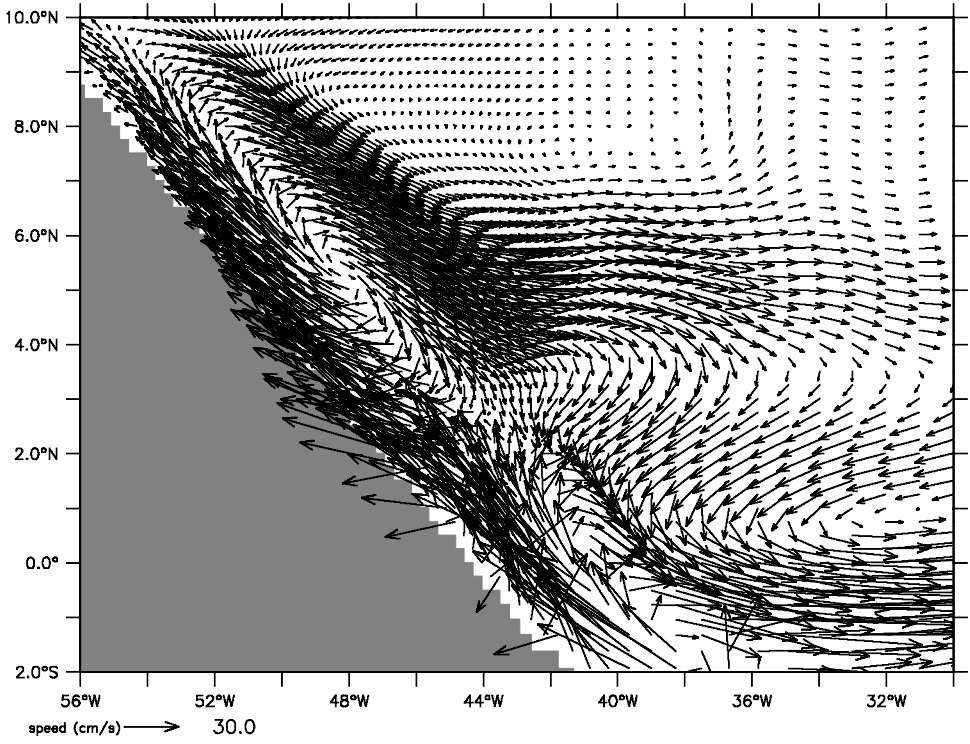

Figure 7. The annual mean flow at 100 m depth. The NBC can be seen flowing northwestern along the coast and feeding the eastward EUC at 2N and the NECC at 7N.

The structure of the flow is very similar to that inferred by Johns et al. (1998) from their current meter moorings (compare with their Fig. 9). The NBC transport at this latitude varies from 9 Sv in March to 36 Sv in July, which once again compares well with the observations of Johns *et al.* (1998). The zonal transport in the upper 300 m between 3N and 9N across 38W has a similar cycle with no transport from April to May and a maximum of 28 Sv in September, very similar to the observations discussed in Katz (1993). This transport contains the NECC transport and the Ekman transport, which cancel each other in late spring. This compensation between the NECC and Ekman transports can be seen in Figure 5, which shows the zonal velocity at 38W in April. Although the NECC flows eastward throughout the year, in spring the transport between 3N and 9N is zero.

The NBC rings also compare well with the observations described in Fratantoni *et al.* (1995), Goni and Johns (2000) and Fratantoni and Glickson (2002). In the model, the NBC rings are shed on average every 50 days and their propagation speed varies from zero to 15 cm/s. At 8.5N the average maximum swirl velocity is 85 cm/s at the surface and the average penetration depth of the 10 cm/s isotach is 650 m +/− 50 m (see snapshots of the NBC rings in Figure 16 and 24). The NBC rings in our simulation seem to be slightly

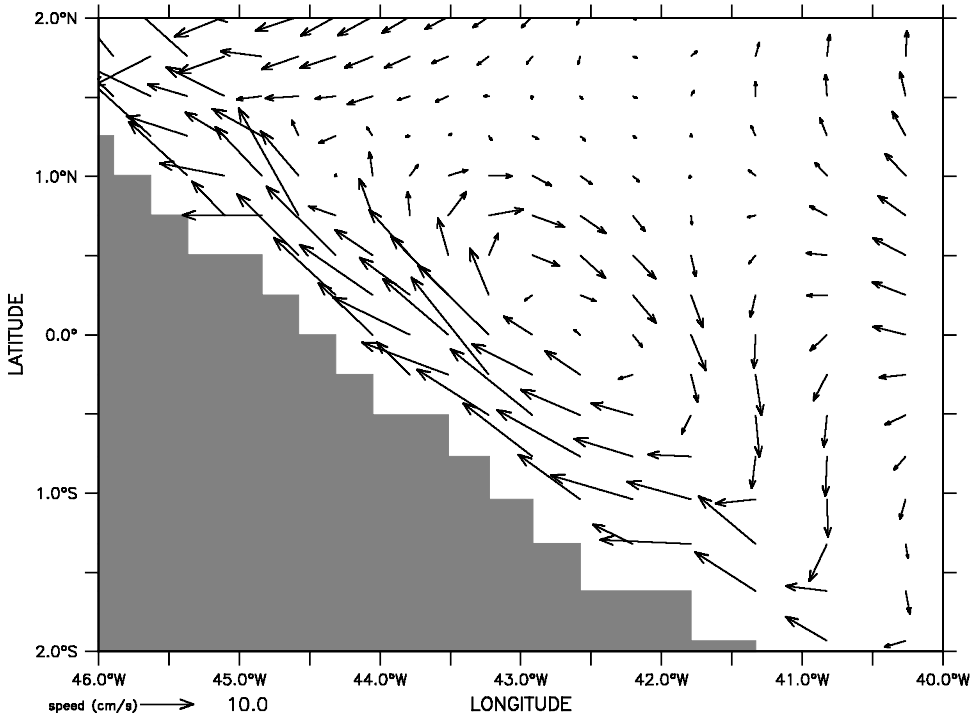

Figure 8. The flow field of an eddy that has been formed by the IWBC at 700 m depth (from MW).

stronger and deeper than the ones generated in the simulation of Fratantoni *et al.* (1995). We attribute this to the higher vertical resolution in our model and a lower viscosity.

The above discussion is by no means a detailed comparison between observations and the present results. Its purpose is solely to demonstrate that the simulation, even though idealized, is able to reproduce reasonably well the NBC rings and the two most important currents of this region, the NECC and the NBC. Three different experiments were performed and will be discussed in the next section: SW is the experiment conducted with seasonal varying wind, MW the experiment with annual mean winds and NW is carried out without winds.

3. Ring shedding

a. Simulation results

In the previous section the properties of the mean circulation were shown to be rather realistic when compared with the observations. This realism gives confidence that the simulations can be analyzed to explore the mechanisms of ring generation. It is helpful to analyze NW (without wind) first. In this experiment the water enters the domain through the southern open boundary, moves north along the western boundary as only there can it

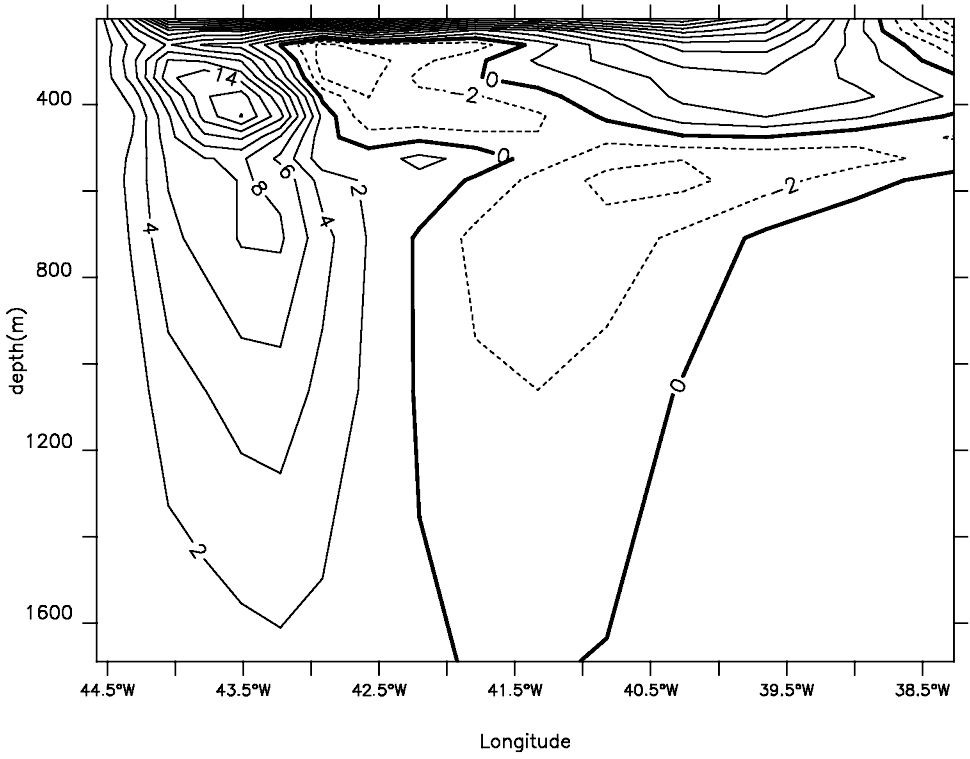

Figure 9. The profile of the meridional velocity in the intermediate eddy of Figure 8 at the equator (in cm/s). The center of the eddy is at 42.5W and it reaches from 400 m down to 1500 m depth.

change its potential vorticity and leaves the basin again through the northern boundary. Near the equator the flow breaks up into eddies (about 6 per year) that propagate northwestward along the coast as shown in Figure 6. This mechanism has been thoroughly analyzed by Edwards and Pedlosky (1998). Upon crossing the equator the sign of the planetary vorticity changes. Outside the frictional boundary layer (20 km wide in this experiment), the flow must change the sign of its relative vorticity to conserve potential vorticity. If the friction is small enough and the inertial boundary layer (60 km wide at intermediate depths) is wider than the frictional boundary layer, a portion of the flow lies outside the frictional boundary layer and the resulting shear causes the flow to become barotropically unstable and to break up into eddies (Edwards and Pedlosky, 1998).

If wind is added as an additional forcing, the surface and thermocline waters may have other means of changing their potential vorticity, as described in the discussion of Killworth's (1991) work later in this section. However, the water below the thermocline will be largely unaffected by the wind (most of the upwelling occurs in the upper 300 m). Therefore, for subthermocline and intermediate flow, which are not distinguished in the

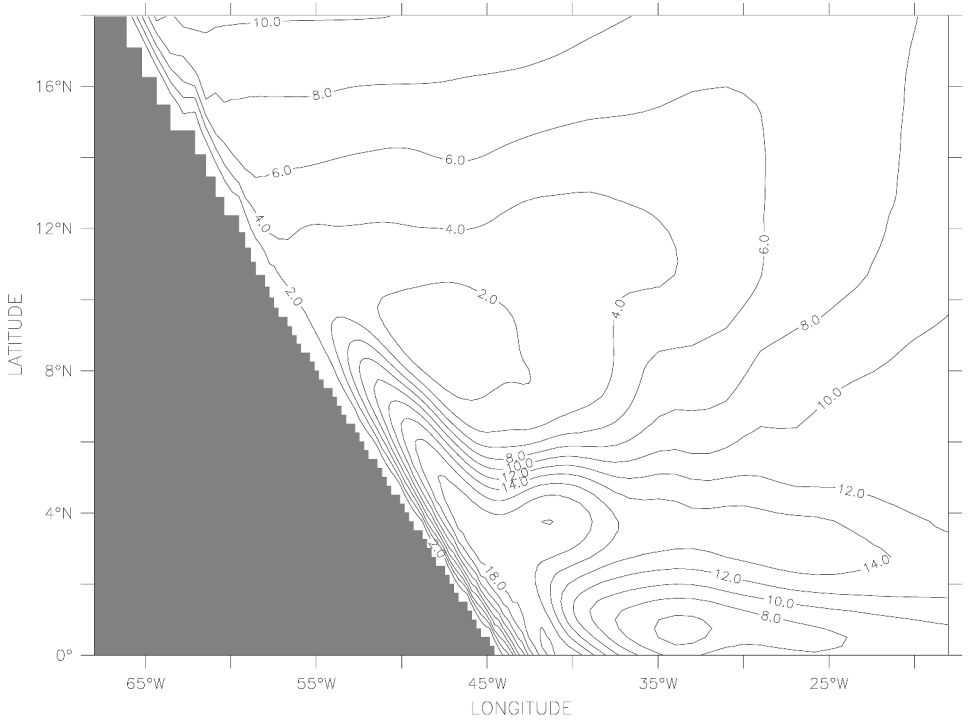

Figure 10. The mean transport in the upper 200 m of the tropical gyre indicated by an approximate streamfunction (in Sv).

present analysis, a similar behavior as for the flow without wind is to be expected. This expectation will be confirmed by the simulations carried out with winds, as shown below.

Observations show that after crossing the equator most of the surface and thermocline water feeds the EUC and the NECC at around 2N and 7N, respectively (Schott *et al.,* 1998). The numerical solution shows that a small part of it enters a recirculation gyre that is part of the NBC/NECC retroflection and is centered at approximately 5N (see Fig. 7). This recirculation gyre is the seed for a NBC ring (as shown observationally by Johns *et al.,* 1990). It is important to note that in SW and MW the flow in the upper layer does not break up into eddies before 4°N. However, as previously discussed, the flow in the intermediate layer breaks up upon crossing the equator. This is shown in Figures 8 and 9 from MW. After the IWBC crosses the equator, an intermediate eddy is generated having a subthermocline width and strength very similar to those of the NBC (Fig. 4). From Figure 9 it can be seen that the eddy's flow field has a coherent structure between 500 m and 1500 m that is very different from the flow above 500 m depth. In both SW and MW there are about 4–5 intermediate eddies created every year. Thus, the intermediate flow can create eddies that have no thermocline expression. The intermediate eddies continue north along the coast with speeds of approximately 10 cm/s.

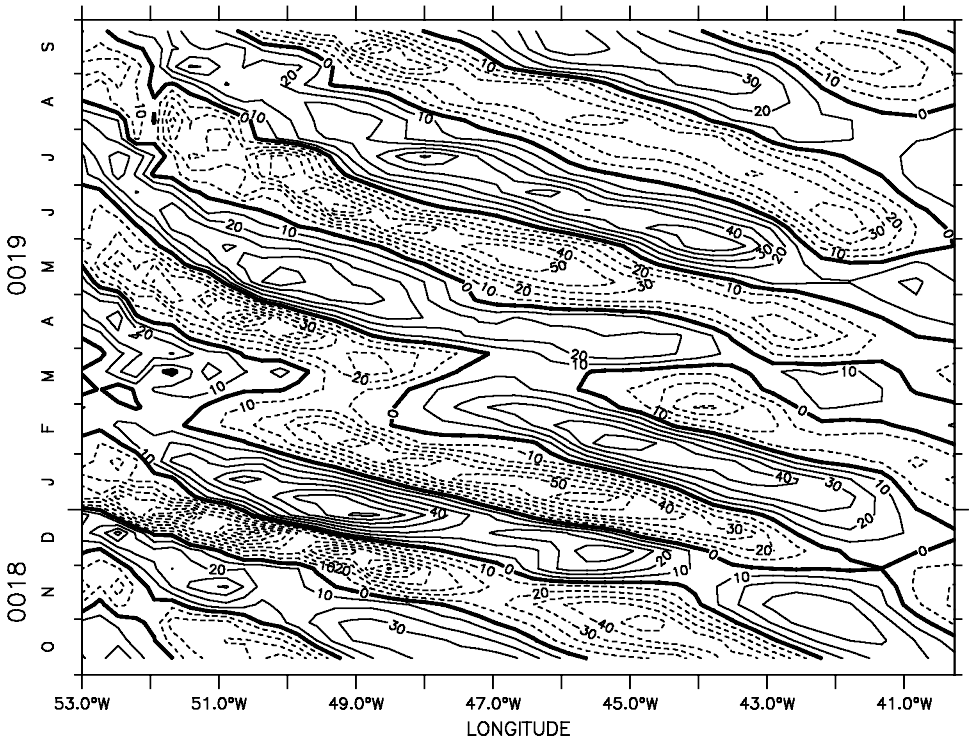

Figure 11. Hovmoeller diagram of the anomalies of the meridional velocity at 6.8N and 100 m depth (in cm/s). The phase speed of those anomalies is approximately −10 cm/s.

Since the flow in the intermediate layer breaks up upon crossing the equator (Fig. 8), the dynamics between the upper layer (0–300 m) and the intermediate layer (300–1000 m) must be different. First, the NBC entrains water with a relatively high potential vorticity from the northern South Equatorial Current that replaces the low potential vorticity water which the NBC lost to the EUC (Schott *et al.,* 1998). Second, the upper layer flow is more nonlinear than the intermediate flow. This can be verified by comparing their Reynolds numbers, defined as UL/A_h where L is the current width. The intermediate layer as a Reynolds number of ~30 with speeds of approximately 10 cm/s whereas the upper layer can reach Reynolds numbers of more than 500 and speeds of up to 2 m/s (see Fig. 4 which shows that even in the mean the flow can reach speeds of 120 cm/s). This suggests that one may treat the upper layer flow as an inviscid system.

Killworth (1991) studied the inviscid adjustment problem for cross equatorial flow and found that a nonlinear flow can penetrate up to two Rossby radii of deformation into the Northern Hemisphere without any adjustment of its potential vorticity. However, to compensate for the lower angular momentum of the higher latitudes, the water has to gain eastward momentum upon flowing northward. This leads to a third major difference

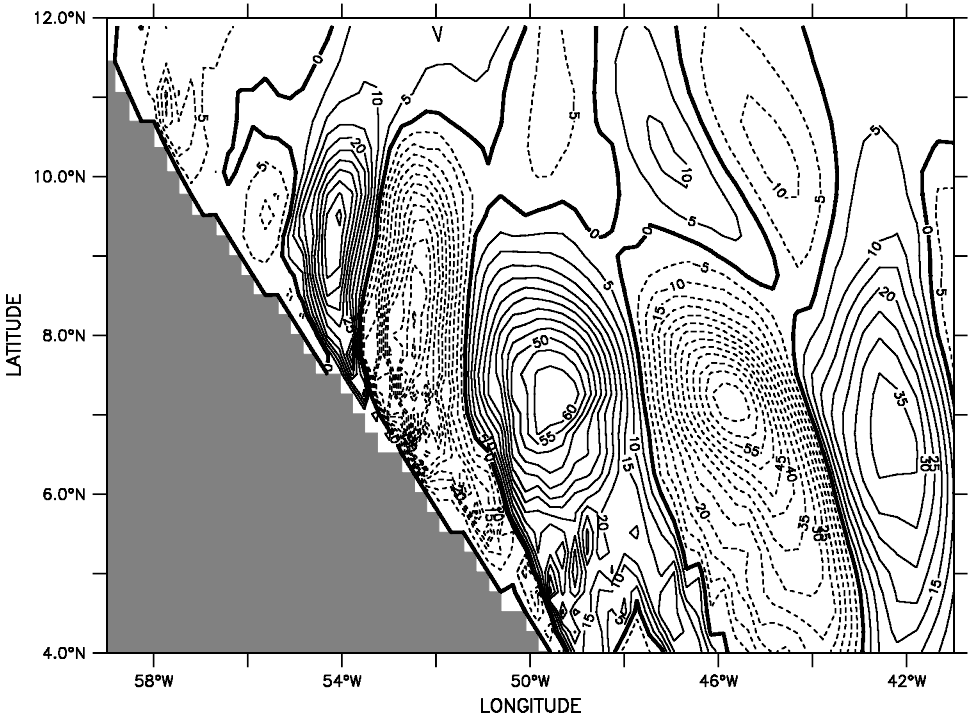

Figure 12. Anomalies of the meridional velocity at 100 m depth (in cm/s). This is an indication of a Rossby wave approaching the coast and reducing its wavelength upon reflection to the north.

between the upper and the intermediate layer. The intermediate layer water has to flow northward not only by two Rossby radii but all the way to the northern boundary where it leaves the basin because of the northern open boundary conditions. On the other hand, the upper layer water has an immediate sink two Rossby radii away from the equator—the wind-driven NECC. Eventually also the upper layer water has to flow northward, but it can do so in the Ekman layer of the tropical gyre where the wind changes its potential vorticity. Figure 10 illustrates this path: the water enters the NECC and then leaves it in the interior to flow northward in the Ekman layer which contains most of the transport of the tropical gyre. This comparison between Killworth's and the present experiments suggests that potential vorticity dynamics is not sufficient to explain the ring generation in the upper layer.

The mechanism of shedding of NBC rings in the present experiments is now discussed. The results from MW (steady winds) will be discussed first. The main differences between SW and MW with regard to the rings are that the rings in SW are more variable in strength and that the generation frequency in the two experiments is slightly different (every 50 days in SW and every 63 days in MW). Ma (1996) proposed the following generation mechanism: a long Rossby wave reflects at the western boundary and creates a short

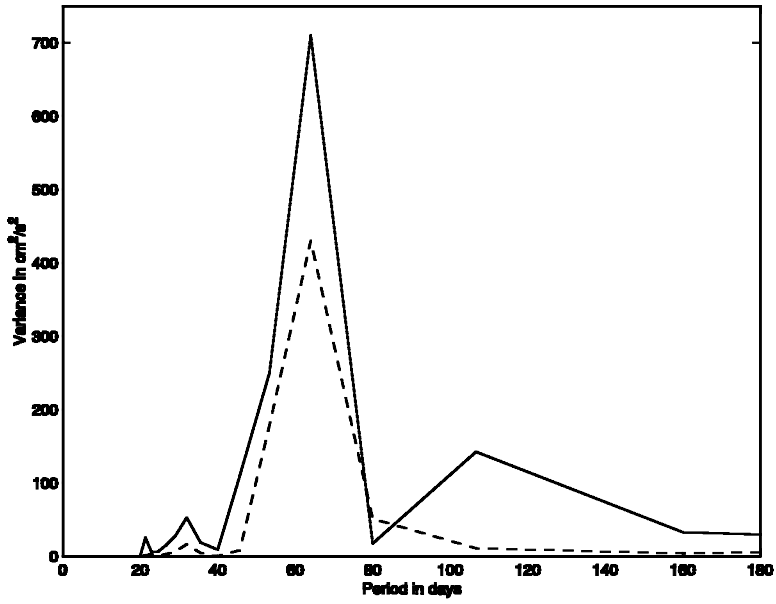

Figure 13. Variance conserving spectrum of the meridional velocity at 6.8N at 100 m depth at 42W (broken line) and 48W (solid line).

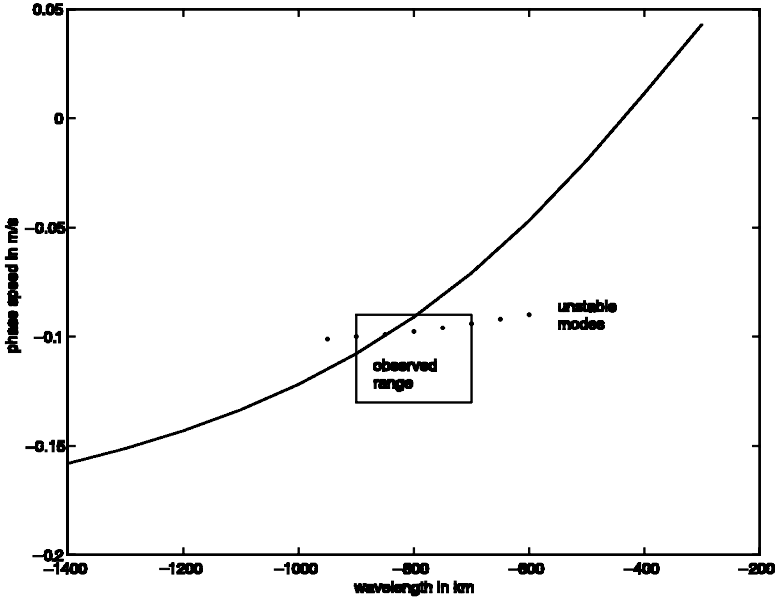

Figure 14. Dispersion relation for a first baroclinic mode Rossby wave with a background velocity of 10 cm/s and a meridional length scale of 1200 km. The box indicates the range of the waves observed in MW and the dots the phase speed of the most unstable modes (see later in the text).

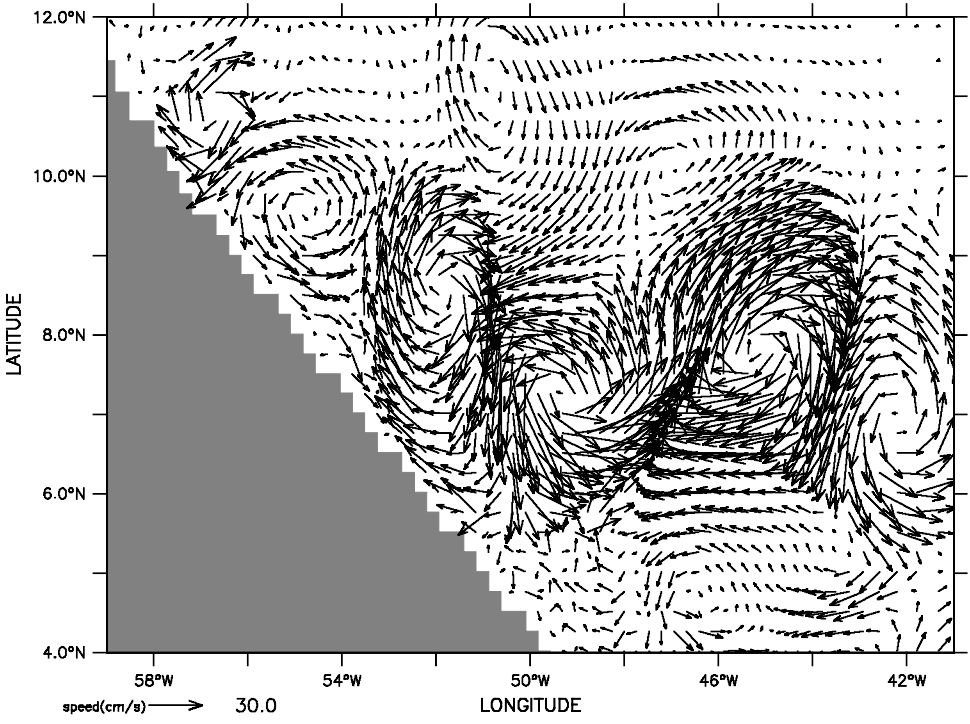

Figure 15. The vectors of velocity anomalies at 10 m depth.

Rossby wave with its characteristically high anomalies in relative vorticity. Due to the β-effect and the interaction with the boundary, those potential vorticity anomalies detach from the reflection region and propagate northwestward along the coast. While this is a qualitative description of what happens in the model, Ma (1996) does not provide a detailed discussion of the process.

A close look at the properties of the dominant waves in the model reveals a phase speed c between -9 cm/s and -13 cm/s, a meridional wavenumber 1 of approximately $2\pi/1200$ km, a zonal wavenumber k between $2\pi/700$ km and $2\pi/900$ km, and a period of approximately 63 days (from the analysis of Figs. 11, 12, and 13 respectively). The background velocity U was calculated by averaging over an area 500 km $\times$ 500 km centered at 7N/44W and estimated to be 10 cm/s.

The wavelength and phase speed of the first baroclinic mode Rossby waves are connected through the dispersion relation:

$$c = \frac{U(k^2 + l^2) - \beta}{k^2 + l^2 + \lambda^{-2}} \tag{1}$$

with $\beta = 2.3e - 11$/ms and the deformation radius of the first mode $\lambda = 115$ km (Pedlosky (1979)). Figure 14 visualizes the dispersion relation and shows the values of

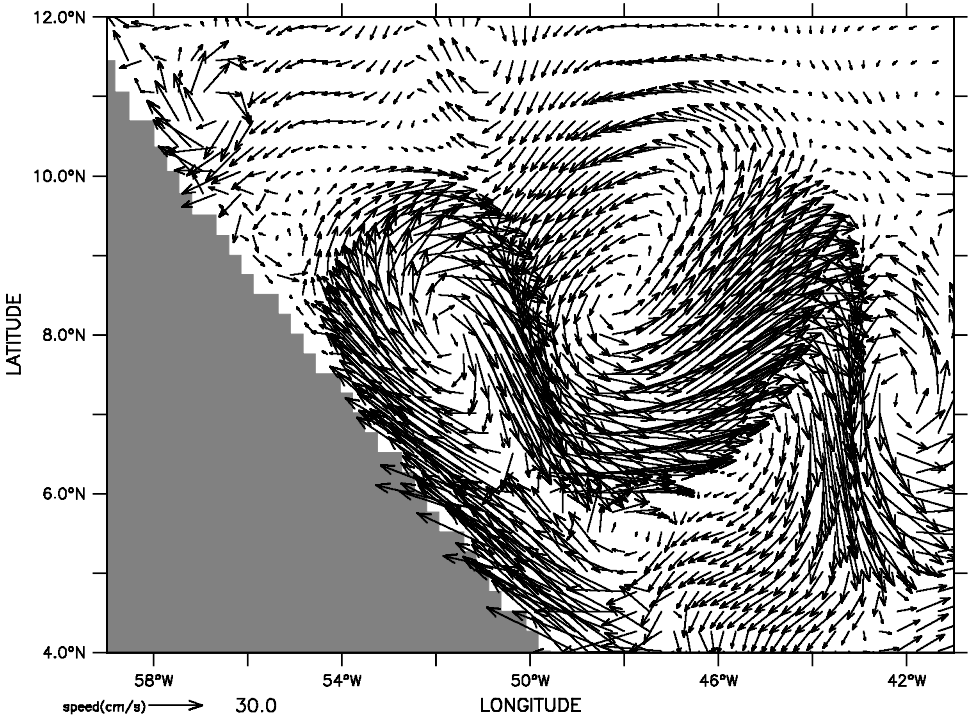

Figure 16. The vectors of absolute velocity for the same time and depth as for the previous figure.

wavelength and phase speed as found in the model. This shows that the model spectrum is dominated by long Rossby waves of the first baroclinic mode. Observational evidence for westward propagating SSH anomalies on the NECC can be found in Leeuwenburgh and Stammer (2001).

The reflection of such a wave at the Brazilian coast is now discussed. Following LeBlond and Mysak (1978), Rossby wave energy is reflected according to Snell's law. This yields the wavenumbers of the reflected wave, and graphically the results can be obtained by using a slowness circle with an inclined coastline. For a Rossby wave with λ_x between 700 km and 900 km and $\lambda_y = 1200$ km, the reflected zonal wavelength would be between 400 km and 500 km. The resulting group velocity would be northwestward along the Brazilian coast. This compares well with the model result of 400 km (Fig. 12). Johns *et al.* (1990) find first mode baroclinic Rossby waves at 8.5N/51.2W, where the reflected wave would already be present, with a timescale of 40–60 days and wavelengths between 390 km and 740 km.

It is difficult to prove that what is observed is indeed a first mode Rossby wave. The background flow and the stratification are by no means uniform, the waves are nonlinear and they are growing while they are propagating westward (Fig. 13). The reflection problem is clearly not straightforward either, because a part of the Brazilian coast is

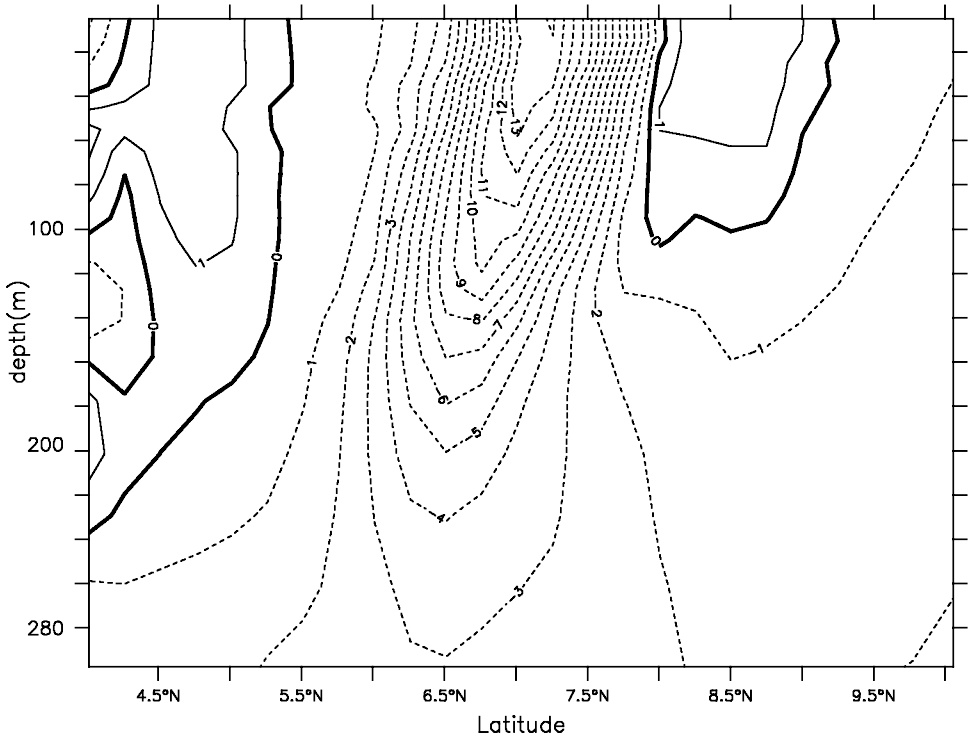

Figure 17. The yearly mean value of $u_{yy} - \beta$ at 46W for MW (scaled with a factor of $1 \cdot 10^{-11}$ $(\text{ms})^{-1}$).

dominated by the strong NBC. However, the close resemblance of the model results with theoretical predictions and observations gives a reasonable confidence in this interpretation.

The relationship between the Rossby waves on the NECC and the NBC rings is now discussed. There are about six NBC rings generated every year as a manifestation of the 63 d period Rossby waves. The analysis of the model results show that indeed every anticyclone sheds a ring. The details of this process are displayed in Figures 15 and 16. Figure 15 shows the velocity anomalies created by a Rossby wave. The wave, which consists of equally strong cyclones and anticyclones, becomes deflected northwestward and propagates along the coast. After reflection, however, the cyclones become weaker and broader than the anticyclones as it can be seen by comparing the anticyclone at 57W with the cyclone at 55W. This behaviour is qualitatively explained by conservation of potential vorticity; the anticyclones intensify to compensate for the increasing planetary vorticity, while at the same time the cyclones must progressively weaken. The intensified anticyclones become NBC rings. It is difficult to observe the cyclones; not only they become weaker as they move northward, they are also superimposed on the strong anticyclonic

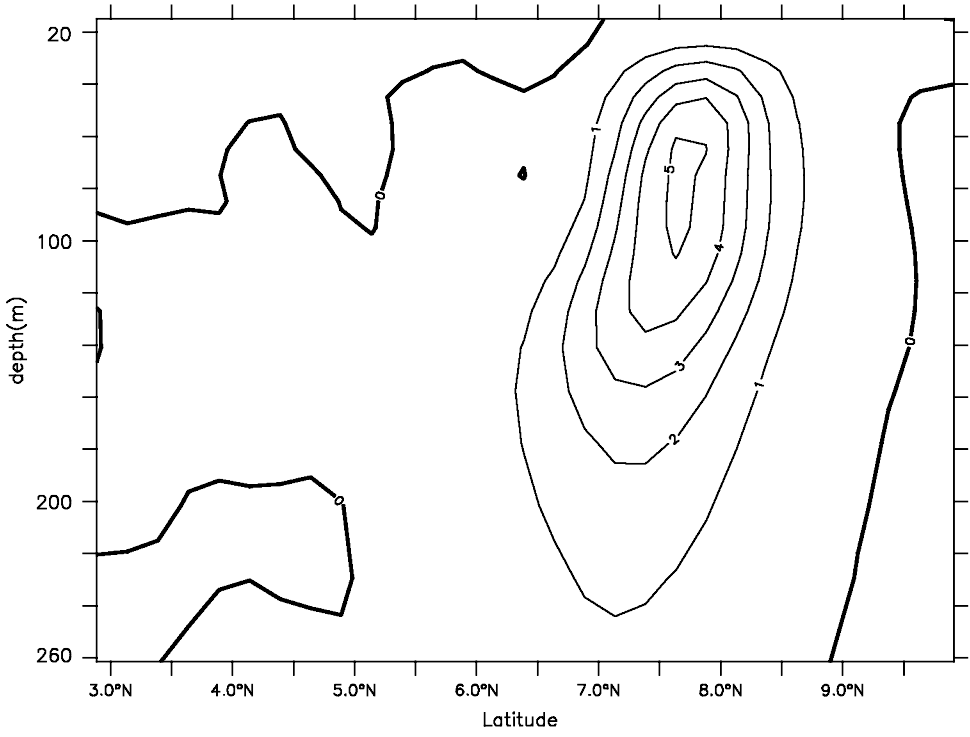

Figure 18. Yearly mean baroclinic conversion averaged between 50W and 42W (contour interval $1 \cdot 10^{-9}$ m^2/s^3). Positive values indicate a flux from eddy available potential energy to eddy kinetic energy.

circulation of the NBC/NECC retroflection. Figure 16 shows in fact that along the Brazilian coast the cyclones are almost impossible to detect in the actual flow.

b. The role of the NECC

Finally, the generation mechanism of the Rossby waves in MW is discussed. MW is chosen because it is the simplest case where the circulation field and the eddy shedding is quasi-steady. At these low latitudes it is difficult to achieve baroclinic instabilities in eastward flowing currents (Pedlosky, 1979, Ch. 7.9); however, the NECC fulfills the necessary conditions for barotropic instability ($u_{yy} > \beta$) in SW (not shown) as well as in MW (Fig. 17). Moreover, the variance of the wave almost doubles while the wave propagates from 42W to 48W as shown in Figure 13. These results are different from those of McClean and Klinck (1995), who found that the NECC in the CME model is not barotropically unstable. The question is then what is the energy source for the Rossby waves. Following Masina *et al.* (1999) the energy flux from eddy available potential energy to eddy kinetic energy (baroclinic conversion, $-g\rho' w'$) and from the mean kinetic energy to eddy kinetic energy (barotropic conversion, $-\overline{u'v'}U_y$) are computed. Figures 18

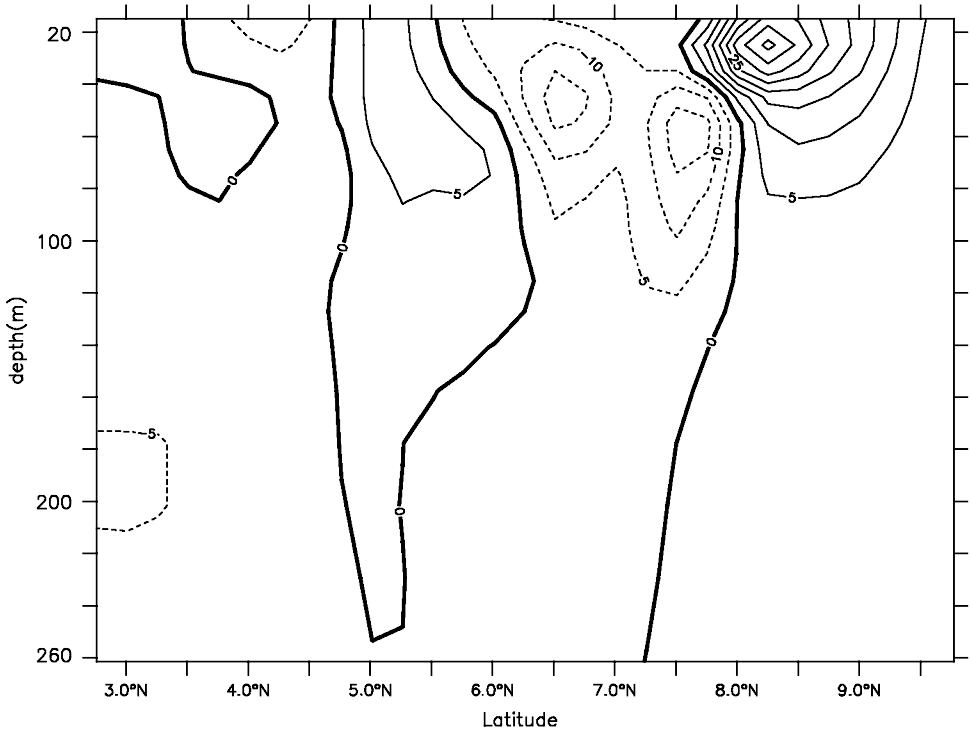

Figure 19. Yearly mean barotropic conversion averaged between 50W and 42W (contour interval $5 \cdot 10^{-9}$ m^2/s^3). Positive values indicate an energy flux from the mean kinetic energy to the eddy kinetic energy.

and 19 show the results. Locally, the baroclinic conversion is an order of magnitude smaller than the barotropic conversion. This strongly suggest that barotropic instability is a generation mechanism for the Rossby waves. However, if the energy fluxes are averaged over the unstable area of the NECC (5N–10N, 50W–42W, 0–100 m), the barotropic conversion averages to $2.0 \cdot 10^{-9}$ m^2/s^3 and the baroclinic conversion averages to $0.7 \cdot 10^{-9}$ m^2/s^3, which shows that baroclinic processes cannot be neglected in the growth of the instabilities.

Further evidence for the instability of the NECC can be obtained through a linear instability analysis. A jet may only be a source of radiating waves if wavelength and phase speed of the instabilities lie on the dispersion curve for a wave in the surrounding medium (Talley, 1983). A linear quasi-geostrophic stability analysis is applied to an idealized model of the NECC to show that the NECC satisfies this radiation condition. In the present experiments the NECC has a Rossby number of 0.2 and the ratio between the average thermocline depth and its meridional deviation is estimated at 0.4. This clearly stretches the validity of the QG approximation, but the strong similarity to be shown between its predictions and the OGCM results gives us confidence in the results.

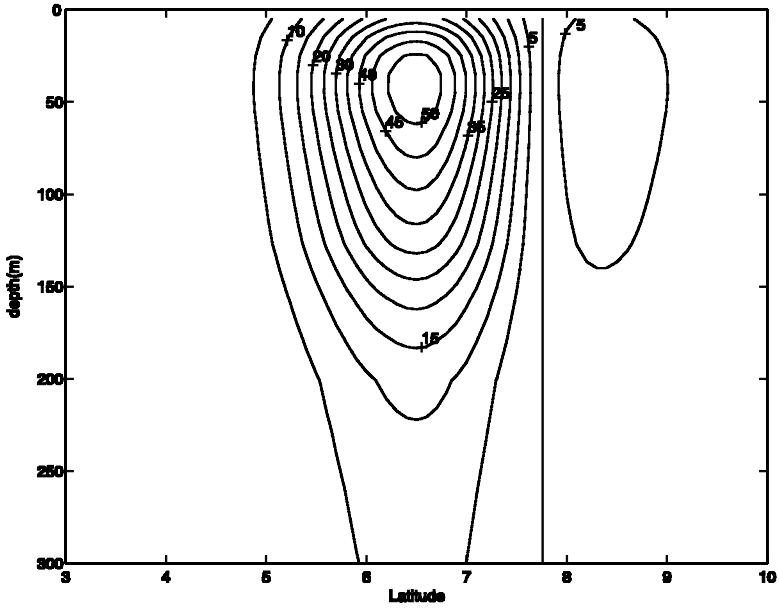

Figure 20. The idealized NECC profile used for the instability analysis. Shown is zonal velocity in cm/s.

The linear form of the QG equations is written in terms of the streamfunction ψ as:

$$\nabla^2\Psi_t + \beta\Psi_x - f_o w_z = 0 \tag{2}$$

$$\Psi_{zt} = (N^2/f_o)w \tag{3}$$

The mean density profile is taken from the model results and the mean NECC profile, shown in Figure 20, is obtained by averaging snapshots of MW. Both profiles should represent the unperturbed state which, of course, is unknown. Therefore we chose profiles that resemble the typical NECC profiles from the model output in terms of stratification, maximum speed, width and depth. The results of the following analysis can be shown to be not overly sensitive to the chosen mean states. These reference density and velocity profiles define a mean streamfunction $\Psi(y, z)$ that together with a perturbation streamfunction $\Phi(x, y, z, t)$ constitute the total streamfunction. Following the average of Beckmann (1988) and Spall (1992), the perturbations are assumed to be wave like:

$$\Phi = M(y)F(z)\exp[i(kx - \omega t)]. \tag{4}$$

Substitution of Eq. (4) into Eqs. (2) and (3) gives an eigenvalue problem for the complex frequency $\omega = \omega_r + i\omega_i$. The system of equations is solved using a second-order finite differences scheme in the horizontal and Chebyshev polynomials in the vertical. Details of the solution procedure can be found in Beckmann (1988). The horizontal grid spacing is

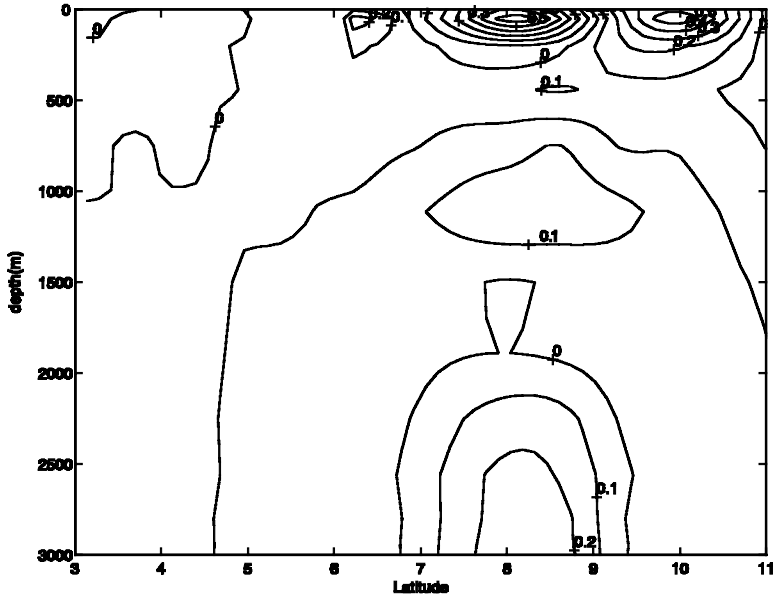

Figure 21. The spatial pattern of the strongest growing mode. Note its vertical structure which resembles a first baroclinic mode and the second maximum at 10N (compare with Fig. 12).

15.6 km and 12 polynomials are used in the vertical. Figure 14 shows the phase speed for the fastest growing westward propagating modes. The predicted values clearly cross the dispersion curve within the observed range. The spatial pattern of the 850 km mode is shown in Figure 21. Its vertical structure compares well with the vertical structure of the first baroclinic mode and its meridional structure predicts the second maximum at 10N (see Fig. 12). The predicted growth rate for an 800 km wave is $2.85 \cdot 10^{-7}\,s^{-1}$ ($\approx$ (40 days)$^{-1}$), and the rates observed in the model are between $2.6 \cdot 10^{-7}\,s^{-1}$ and $6.5 \cdot 10^{-7}\,s^{-1}$. As in the previous subsection it is clear that the simulated flow field is more complex than the one analyzed here. Nevertheless the strong similarity between the theoretical prediction and the model results justifies this approach.

c. The deep structure of the rings

A recently concluded observational campaign, the NBC Rings Experiment (Wilson *et al.,* 2002) showed that the NBC rings can reach well below the thermocline. The retroflection does not reach below the thermocline and has its maximum velocity near the surface. Thus, the mechanism discussed in the previous section is not sufficient to explain the deep structure of the NBC rings. The model results suggest that the deep signal can be explained by the merger of a deep intermediate eddy (see Section 3a) with the retroflection eddy. Figure 22 shows four successive snapshots of negative relative vorticity for SW in two layers, the solid lines being contours of ζ at 100 m depth and the broken line contours

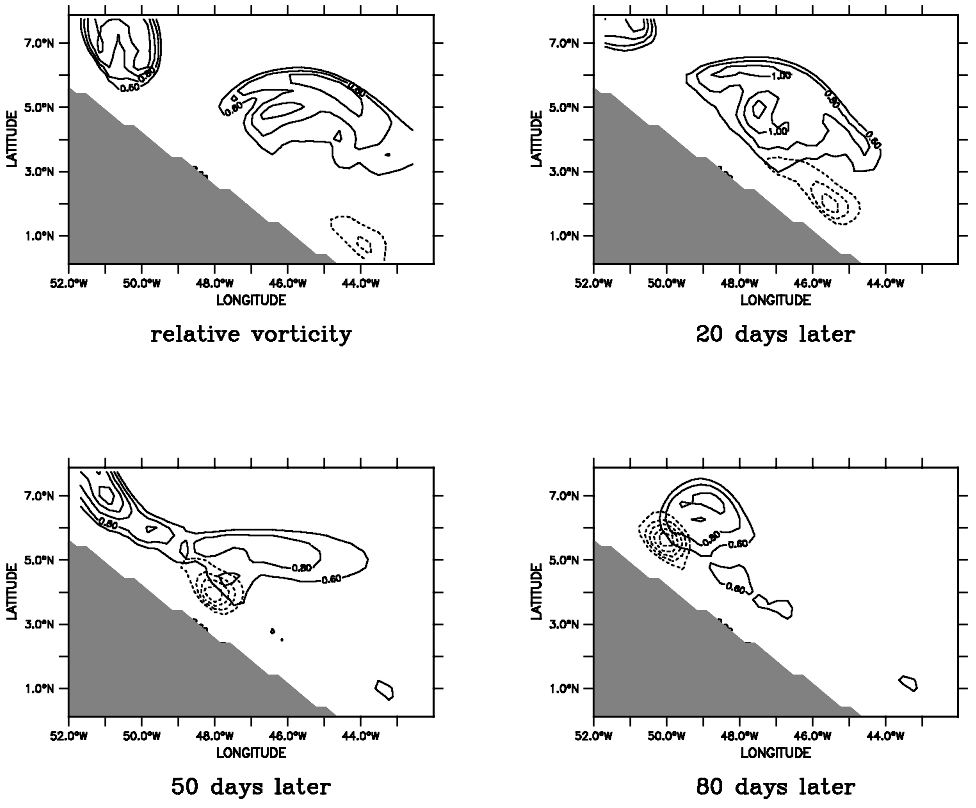

Figure 22. Four successive snapshots of negative relative vorticity (ζ) to illustrate the merger of an intermediate eddy with the shallow retroflection ring. The solid lines show ζ in 100 m depth between $-0.6 \cdot 10^{-5}$ s^{-1} and $-1.4 \cdot 10^{-5}$ s^{-1}. The broken lines show ζ in 700 m depth with each contour indicating $-0.2 \cdot 10^{-5}$ s^{-1}.

of ζ at 700 m depth. The negative relative vorticity indicates anticyclones: the retroflection eddy at 100 m and the intermediate eddy at 700 m. One can see in this figure how the intermediate eddy (see Figs. 8 and 9) travels north along the coast and becomes stronger to balance for the increasing planetary vorticity. Eventually it merges with the retroflection eddy. Figure 23 shows the shallow retroflection eddy before the merger, with only a very weak signal below the thermocline. This changes after the merger when the newly created NBC ring shows a strong signal beyond 100 m as shown in Figure 24. Even though there are about 4–5 intermediate eddies generated per year, only 1 or 2 of them propagate northward beyond 5N while the others dissipate on the way.

This experiment shows that shallow NBC rings can merge with intermediate eddies. The details of the interaction between the eddies before and during the merger have not been examined, because such an analysis would require a simpler, more idealized approach, for instance with a 2 layer model.

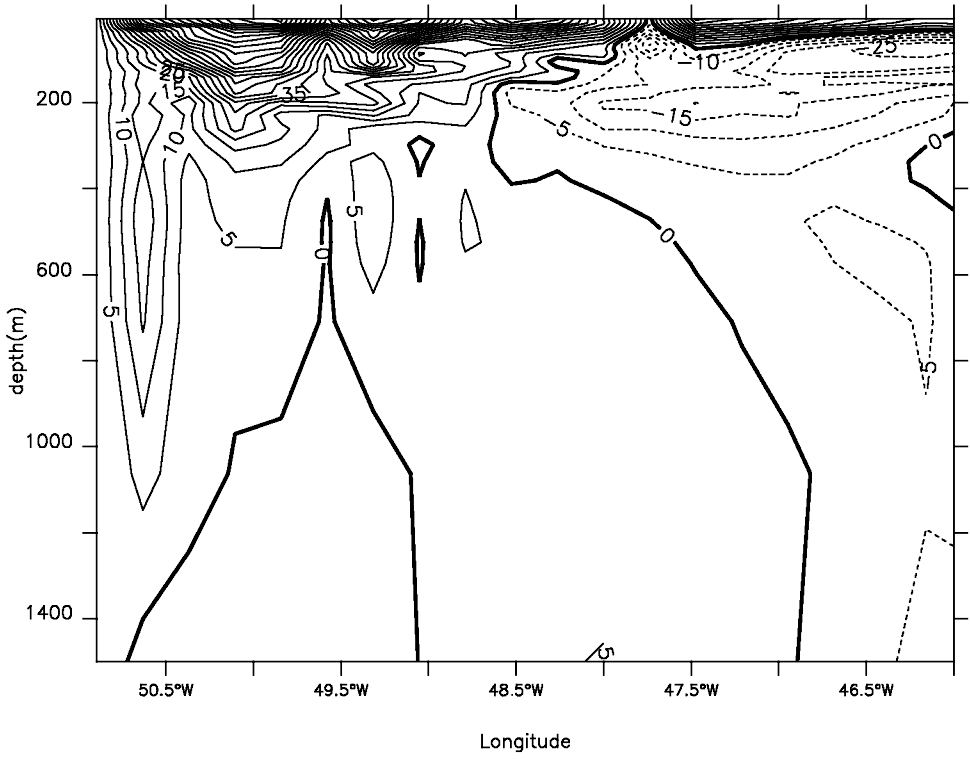

Figure 23. Contours of meridional velocity across the shallow retroflection ring at 5N (contourlines every 5 cm/s). This snapshot was taken 40 days after the first ζ plot of Figure 22.

4. Summary and conclusions

The focus of the present investigation has been on explaining the generation mechanisms of NBC rings and their vertical structure, capitalizing on the available observational evidence and on previous modeling studies. An idealized OGCM of the tropical Atlantic was used which is able to reproduce the basic features of the tropical Atlantic circulation as well as the NBC rings.

Three numerical experiments were carried out, one without winds and two including the wind effects, either steady or including the seasonal cycle. In NW, without winds, the NBC current flows northwestward along the western boundary where it can change its potential vorticity. As explained in Edwards and Pedlosky (1998), if the inertial boundary layer is broader than the frictional one, the flow outside the frictional boundary layer must change the sign of its relative vorticity to conserve potential vorticity, thus it becomes unstable and breaks up into eddies. With the vorticity input provided by the wind, the surface and thermocline current does not become unstable and the flow does not break up. Both with steady winds (MW) and with variable ones (SW), a consistent, unique scenario emerges for the generation of NBC rings.

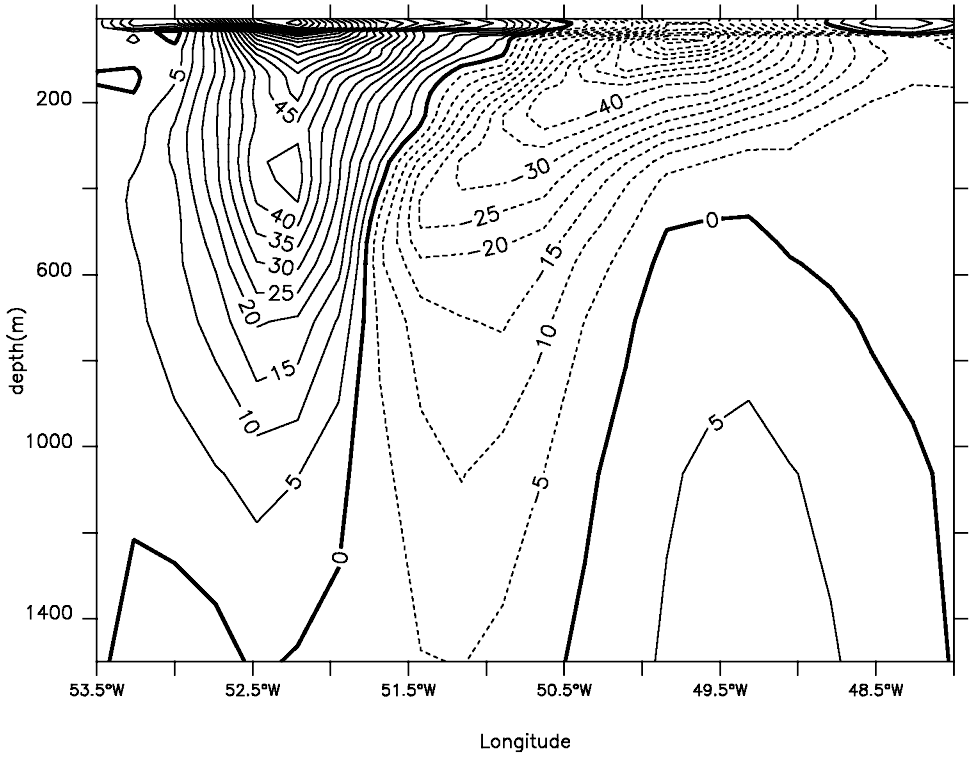

Figure 24. Contours of meridional velocity across the NBC ring of Figure 22 (7N, after a 100 days) after the merger (contourlines every 5 cm/s).

First, it is shown that the NECC is barotropically unstable, radiating Rossby waves of the first baroclinic mode with a period of about 63 days in MW and of 50 days in SW. These waves reflect at the Brazilian coast creating about six anticyclones per year in MW and seven in SW. Among these NBC rings, about one per year reaches a depth below 1000 m. These deep rings are created by the merger of a surface NBC ring with an intermediate eddy, produced by the instability of the IWBC. The main difference between SW and MW is that, with variable winds, the ring generation frequency is slightly higher and they are more variable in strength.

Even though with the present model configuration the generation of NBC rings can be studied and explained, the resolution used is too coarse to study the details of the decay process. A general statement can however be made. As shown by Anderson and Corry (1985), the tropical gyre spins up and down in phase with the tropical wind. As a consequence, the propagation speed of rings is modulated by the seasonal cycle of the wind field. Although this does not affect the generation frequency, the resulting background flow accelerates or decelerates the rings, and the modulation determines for how long the rings are exposed to dissipative processes before they cross the boundary between the tropical

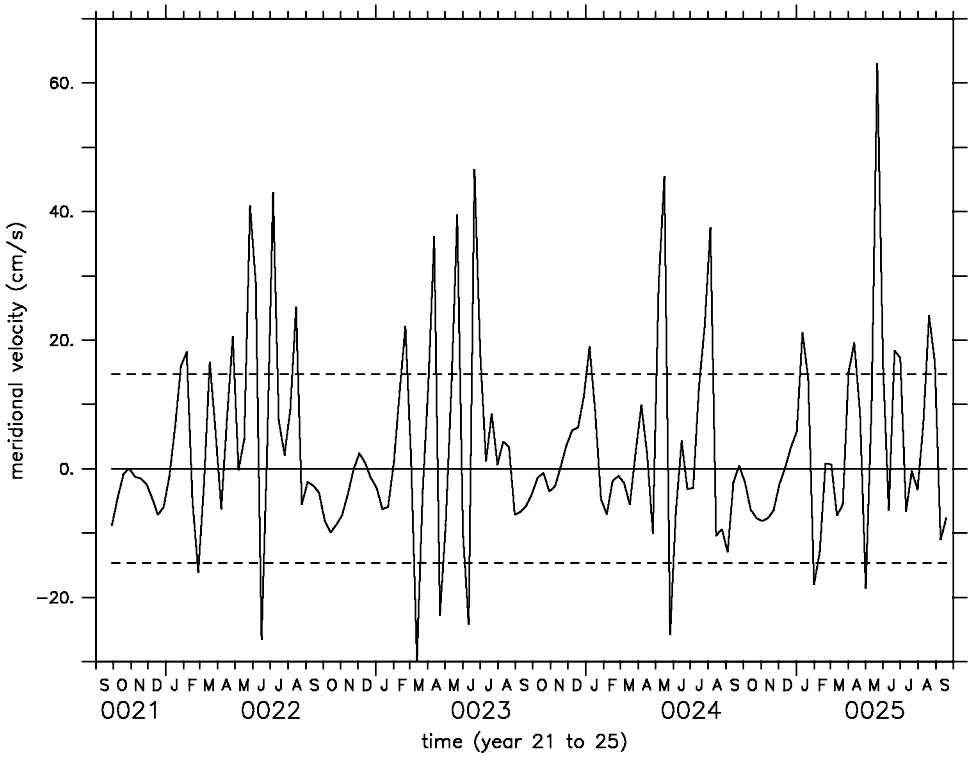

Figure 25. 4 year time series of meridional velocity (in cm/s) at 10N/56W in 100 m depth (for SW). The broken lines indicate the standard deviation around the mean. NBC rings can be identified as peaks above or below the standard deviation. One can see that NBC rings preferentially pass by 10N in the late spring at an average rate of approximately 3–4 rings per year.

and subtropical gyres. In the time series of meridional velocity at 10N/56W and 100 m depth shown in Figure 25; the NBC rings can be identified as peaks above or below the standard deviation around the mean, marked by straight lines. Even though rings are generated every 50 days, the period of the first baroclinic mode in SW, only about 3 to 4 rings per year reach as far as 10N, preferably in late spring.

The question of whether NBC rings are an important contributer to the upper warm limb of the MOC in transporting northward southern Atlantic water cannot be answered by the present study and remains an open one. The observational study by Fratantoni *et al.* (1995) gives a value of 3 Sv as the lower bound for the southern Atlantic water transported northward by the rings. This value is much higher than the transport we estimate from SW on the basis of 3–4 rings passing through 10N per year and on the basis of their vertical structure in the simulations. For this transport we have values ranging from 0.8 Sv to 1.8 Sv. Various reasons may account for this difference, the most important one being that the rings generated in the simulations rarely reach penetration depths greater than 1000 m,

while the transport evaluated by Fratantoni *et al.* (1995) is based on observations containing deep rings, with penetration depths well beyond 1000 m. According to our explanation of the deep structure of the rings, one could argue that the water below the thermocline always flows northwards. Whether it does so in a ring or in the IWBC may not be so important as far as the MOC return flow is concerned. Regarding the study of the rings decay process, a higher resolution, both in the vertical and the horizontal, is necessary to obtain a more realistic representation of the relevant processes.

Acknowledgment. The authors are thankful for the useful comments of Bill Johns and Dave Fratantoni. Furthermore they benefitted from the helpful suggestions of Tony Busalacchi, Glenn Flierl, Breck Owens and Mike Spall. Aike Beckmann is thanked for providing the solution procedure for the linear stability analysis and Arne Biastoch for help with the open boundary conditions. The computations have been performed at the NCAR facilities in Colorado and this research was funded with NASA grant NAG5-7194 and with NOAA grant NA16GP1576 at MIT.

REFERENCES

Anderson, D. L. T. and R. A. Corry. 1985. Seasonal transport variations in the Florida straits: a model study. J. Phys. Oceanogr., *15,* 773–786.

Beckmann, A. 1988. Vertical structure of midlatitude mesoscale instability. J. Phys. Oceanogr., *18,* 1354–1371.

da Silveira, I. C. A., W. Brown and G. Flierl. 2000. Dynamics of the North Brazil Current Retroflection region from the WESTRAX Observations. J. Geophys. Res. (submitted).

Didden, N. and F. Schott. 1993. Eddies in the North Brazil Current retroflection region as observed by GEOSAT altimetry. J. Geophys. Res., *98,* 20121–20131.

Edwards, C. A. and J. Pedlosky. 1998. Dynamics of nonlinear cross-equatorial flow. Part I: potential vorticity transformation. J. Phys. Oceanogr., *28,* 2382–2406.

Fratantoni, D. M. and D. A. Glickson. 2002. North Brazil Current ring generation and evolution observed with SeaWiFS. J. Phys. Oceanogr., *32,* 1058–1074.

Fratantoni, D. M., W. E. Johns and T. L. Townsend. 1995. Rings of the North Brazil Current. J. Geophys. Res., *100,* 10633–10654.

Goni, G. J. and W. E. Johns. 2000. A census of North Brazil Current rings observed from TOPEX/POSEIDON Altimetry: 1992–1998. Geophys. Res. Lett., *28,* 1–4.

Hellerman, S. and M. Rosenstein. 1983. Normal monthly wind stress over the world ocean with error estimates. J. Phys. Oceanogr., *13,* 1093–1104.

Johns, W. E., T. N. Lee, R. C. Beardsley, J. Candela, R. Limeburner and B. Castro. 1998. Annual cycle and variability of the North Brazil Current. J. Phys. Oceanogr., *28,* 103–128.

Johns, W. E., T. N. Lee, F. Schott, R. J. Zantropp and R. H. Evans. 1990. North Brazil Current retroflection: seasonal structure and eddy variability. J. Geophys. Res., *95,* 22103–22120.

Jochum, M. and P. Malanotte-Rizzoli. 2001. On the influence of the meridional overturning circulation on the tropical-subtropical pathways. J. Phys. Oceanogr., *31,* 1313–1323.

Katz, E. J. 1993. An interannual study of the North Equatorial Countercurrent. J. Phys. Oceanogr., *23,* 116–123.

Killworth, P. 1991. Cross-equatorial geostrophic adjustment. J. Phys. Oceanogr., *21,* 1581–1601.

LeBlond, P. H. and L. A. Mysak. 1978. Waves in the Ocean, Elsevier, 602 pp.

Leeuwenburgh, O., and D. Stammer. 2001. The effect of ocean currents on sea surface temperature anomalies. J. Phys. Oceanogr., *31,* 2340–2358.

Liu, Z. and S. G. H. Philander. 1995. How different wind stress patterns affect the tropical-subtropical circulations of the upper ocean. J. Phys. Oceanogr., *25,* 449–462.

Ma, H. 1996. The dynamics of the North Brazil Current retroflection eddies. J. Mar. Res., *54,* 35–53.
Masina, S., S. G. H. Philander and A. B. G. Bush. 1999. An analysis of tropical instability waves in a numerical model of the Pacific Ocean—2. Generation and energetics of the waves. J. Geophys. Res., *104,* 29613–29635.
McClean, J. L. and J. M. Klinck. 1995. Description and vorticity analysis of 50-day oscillations in the western tropical region of the CME Model. J. Phys. Oceanogr., *25,* 2498–2517.
Oliger, O. and A. Sundstrom. 1978. Theoretical and practical aspects of some initial boundary value problems in fluid dynamics. J. Appl. Math., *35,* 419–446.
Pedlosky, J. 1979. Geophysical Fluid Dynamics. Springer, 707 pp.
Schmitz, W. J. and M. S. Mcartney. 1993. On the North Atlantic circulation. Rev. Geophys., *31,* 29–49.
Schott, F. A., L. Stramma and J. Fischer. 1998. Transports and pathways of the upper-layer circulation in the western tropical Atlantic. J. Phys. Oceanogr., *28,* 1904–1928.
Spall, M. A. 1992. Rossby wave radiation in the Cape Verde Frontal Zone. J. Phys. Oceanogr., *22,* 796–807.
Spall, M. A. and A. R. Robinson. 1989. A new open ocean, hybrid coordinate primitive equation model. Math. Comp. Simulation, *31,* 241–269.
Stevens, D. P. 1990. On open boundary conditions for three dimensional primitive equation ocean circulation models. Geophys. Astrophys. Fluid Dyn., *51,* 103–133.
Talley, L. D. 1983. Radiating instabilities of thin baroclinic jets. J. Phys. Oceanogr., *13,* 2161–2181.
Wilson, W. D., W. E. Johns and S. Garzoli. 2002. Velocity structure of North Brazil Current Rings. Geophys. Res. Lett., *29*(8), 1273.

Received: *26 September, 2002;* revised: *21 March, 2003.*